Journal of Marine Science and Technology (2022) 27:92–103
https://doi.org/10.1007/s00773-021-00817-x

ORIGINAL ARTICLE

Distortion model design of flexible marine riser

Jixiang Song[1,2] · Weimin Chen[1,2] · Shuangxi Guo[1,2] · Dingbang Yan[1,2]

Received: 22 May 2020 / Accepted: 11 April 2021 / Published online: 22 April 2021

Abstract
With the development of deep-sea oil and gas resources, the aspect ratio of deep-sea flexible riser has reached the order of 10^2–10^3, which makes the experimental model of the equal scale of deep-sea flexible risers challenging to achieve under typical experimental conditions. Alternatively, the non-scale experiment is sometimes used. However, the dynamic response of the prototype may not be exactly modeled. To solve the problem, this paper expands the distortion similarity method to consider the pretension and designs a distortion model of the deep-sea flexible riser based on the improved distortion similarity method. Applying the governing equation and dimensional analysis method to analyze the prototype and experimental model, the design method of the distortion model is obtained. In the numerical analysis, the design of the distortion model of a top tensioned riser (TTR) is carried out, and the selection criteria and range of the aspect ratio are proposed. The three parts of the natural frequency similarity, the pretension non-satisfaction similarity, and the error analysis are studied. This analytical study indicates that the transverse direction of the distortion model satisfies the similarity of the dynamics, and the longitudinal direction satisfies the static similarity. The selection of the aspect ratio of the distortion model should satisfy three factors.

Keywords Deep-sea flexible marine riser · Distorted models · Error analysis · Dynamic similarity

1 Introduction

The riser acts as an essential connecting channel between the upper floating body and the subsea wellhead. As the development of marine oil and gas resources moves from shallow sea to deep sea, its length also increases rapidly. When the diameter of the riser is constant, the aspect ratio even reaches 10^2–10^3, which leads to the increase of the flexibility of the riser, and the mode of the structure exhibits low frequency and dense characteristics. Under complex loads, the dynamic response of a deep-sea flexible riser is more complicated than that of a rigid riser [1]. A riser with a length-to-diameter ratio below 10^2 is a rigid riser [2]. Some complex problems such as broadband random vibration, high-order multi-mode frequency locking, and vortex-induced vibration cannot directly obtain theoretical solutions. To study the complex structural dynamic response of flexible risers, experimental observation is needed. However, the length of flexible marine risers is usually in the order of 10^3 m, and the aspect ratio is between 10^2 and 10^3. It is challenging to realize the equal scale experimental model of 10 m or more under laboratory conditions.

Flexible riser experiments are usually divided into prototype experiments, similar experiments (completely similar), and incompletely similar (partially similar) experiments. Prototype experiments (field tests) have fewer applications in practice due to the complexity of the experimental structure, the cost, and the high degree of proprietary [3, 4]. In the similar experiment (equal scale model experiment), the model length is 10 m and above [5–8], and the experimental model of Yin et al. [8] is as short as 9 m, but with a 1:19 scale, the prototype length is the only 171 m. Because the general experimental conditions cannot be met, the number of applications of this experimental model is limited in practice.

Incompletely similar experiments usually ignore the length of the riser and the aspect ratio [9–15], mainly to study the vortex-induced vibration (VIV) and suppression

✉ Weimin Chen
wmchen@imech.ac.cn

[1] Key Laboratory for Mechanics in Fluid Solid Coupling Systems, Institute of Mechanics, Chinese Academy of Sciences, Beijing 100190, China

[2] School of Engineering Sciences, University of Chinese Academy of Sciences, Beijing 100049, China

VIV. Some scholars believe that the riser length only affects whether the high-order mode of the model can be excited in the experiment [10], so the riser length is ignored.

Among the design methods of incompletely similar experiments, the representative is the design method of Vandiver [16]. To study the VIV of the flexible riser, Vandiver proposed a high-order (above 10th order) vortex-induced vibration experimental design method. A problem is in this method that the pretension of the model is not similar to the pretension of the prototype because the angle between the fixed end and the vertical line is limited by applying a considerable pretension. The pretension of this model is much larger than that calculated by similar theory, so it is difficult for the model to predict the dynamic response of the prototype.

Similar problems exist in other experiments [14, 15, 17, 18]. Tognarelli et al. [14] controlled the pretension to make the lateral vibration of the riser reach eighth order, so the pretension does not satisfy the similar theory. Chaplin et al. [15] studied the VIV of the pretensioned riser under gradient flow, and the value of the pretension of the riser model was not determined by similar theory. It can be seen that the incomplete similarity experiment not only ignores the length–diameter ratio of the prototype but also ignores the similarity of the pretension, which only makes the model parameters satisfy the characteristics of the prototype [14, 18], such as mass ratio and Reynolds number reaching 10^5 orders of magnitude.

To solve the problem that the riser dynamics are not similar due to the model aspect ratio and pretension dissimilarity, this paper applies the distortion model method to design the riser model. When the ratio of the geometry of the prototype (P) to the model (M) in the three-dimensional direction is no longer a fixed value, but different value, the model (M) is called a distortion model [19]. The distortion model solves the problem of excessive length-to-diameter ratio of the flexible riser using different geometric scales. Baker et al. [20] first put forward the concept of the distortion model and studied the problem of the drop height of the cantilever plate and the permanent deformation length of cantilever plate through drop test. It is proved that the permanent deformation length of cantilever plate can be similar by the distortion model whose drop height does not satisfy the equal ratio length scale. Since then, many scholars have extended the similarity of distortion models to other structures. For example, the distortion similarity of response parameters such as displacement, buckling load and natural frequency of shell, composite plate, and cantilever plate [19, 21–23], and concluded that the prototype and the model have similarities.

Simitses, Simitses et al. [21] studied the distortion similarity of the displacement, buckling load, and natural frequency of simply supported composite plates, and discussed the distortion similarity of the buckling load of the shell structure. Rezaeepazhand, Rezaeepazhand et al. [22] analyzed the natural frequencies of two configurations of angle-ply laminates and cross-ply laminates. They used the governing equation to derive five similar equations of natural frequency and discussed the similarity errors of the natural frequency of the distortion model of the number of plies and material property change. The results show that the distortion model can also predict the natural frequency of the prototype well. Subsequently, the distortion model is used to study the vibration response of orthogonal cylindrical shells [23] in advanced composite structures. The effects of parametric distortion, such as the number of plies, stacking sequence, length, and radius of the cylinder on the natural frequencies are analyzed. The results show that the parametric distortion models, such as the number of plies and the length and radius of the cylinder can effectively predict the natural frequencies. Luo et al. [19] evaluated the application of the geometric distortion model in predicting the natural frequency of the cantilever plate by governing equations and sensitivity analysis and proposed a scaled model of the distortion model with the same order of the first six modes. The calculation of the approximate and accurate distortion model is carried out. The similarity between the vibration shape and the natural frequency is numerically analyzed. Finally, the effectiveness of the method is verified by experiments. Adams et al. [24] proposed scaling laws by a power law. The power law is directly deduced from the II-theorem of similitude theory and the coefficients of the power law are obtained from first-order sensitivities (sensitivity-based scaling laws). Then, the applicability of the sensitivity-based scaling laws is demonstrated in three case studies. Franco et al. [25] extended the applicability of some similitude laws, developed for thin flat plates under a turbulent boundary layer load, to ribbed plates forced by the same wall pressure fluctuations. At last, a simple approach is proposed to circumvent the distortion effects. Luo et al. [26] proposed a method for deriving the scaling laws of rotor systems based on the generalized equations of subsystems, where gravitational acceleration, geometric, and material distortion are considered. The accuracy and effectiveness of the proposed method are verified by the prediction of the dynamic characteristics of the rotor system. It is found that there is a certain error in the prediction of vertical vibration response by neglecting the gravity acceleration. Casaburo et al. [27] reviewed as possible about similitude methods applied to structural engineering and their limitations due to size effects, rate sensitivity phenomena, etc. After a brief historical introduction and a more in-depth analysis of the main methods, the similar applications are classified.

In summary, according to the author's knowledge, the distortion model of the existing experiments does not consider the effect of pretension. However, the flexible marine riser has the pretension effect, so this paper expands the distortion

similarity method to consider the pretension and apply the improved distortion similarity method designed the distortion model of the flexible marine riser with pretension. The experimental design of the riser is to solve the problem that the riser dynamics of the model are not similar due to the excessive length-to-diameter ratio and the pretension dissimilarity so that the dynamics of the flexible riser are similar. The structure of the article is as follows, Sect. 2, using the theory of elastic mechanics to prove the feasibility of the distortion model. In Sect. 3, the distortion model of the TTR is designed by governing equations and dimensional analysis. In Sect. 4, the numerical analysis method is used to design the distortion model of a flexible marine riser, and the selection range of the aspect ratio is given. The natural frequency of the model verifies the validity of the distortion model. The model and prototype of the pretension similarity are analyzed. The similarity effect of the natural mode, the error analysis of the design model and the experimental model are applied to the natural frequency. The final conclusion is in Sect. 5.

2 Dynamic differential equations of distorted model

From the perspective of the elasticity theory, whether there is a dynamic similarity between the scaled model, with multiple length scale ratios, and prototype is a question. First, in view of the characteristics of the flexible marine riser, the following assumptions are made:

1. The axial deformation and the radial deformation are independent of each other and do not affect each other, that is, the Poisson's ratio is ignored.
2. The differential equation of motion ignores the inertial force in the direction of the distortion.

Hypothesis 1 is based on the linear elastic state of the riser when it is in service. The pretension produces considerable axial stress of the riser, and the riser bending stress caused by the lateral displacement is small, and the difference between the two is enormous. Take the 682.75 m long riser of the Norwegian DeepWater Program [4] as an example. The specific parameters are listed in Sect. 4. The axial stress of the vertical pipe caused by the pretension is 155.2 MPa. It is assumed that the amplitude of the modal vibration is the same as the diameter of the riser. The amplitude of the VIV of the riser is generally considered to be equal to the diameter of the riser, or other values [28]. The stress formula $\sigma_{\max} = 1/2 * D * D_{\text{amplitude}} * (n\pi/L)^2 E$, where D is the diameter of the riser, $D_{\text{amplitude}}$ is the amplitude, which is equal to the diameter D, n is the nth order mode number, L is the length of riser, E is the elastic modulus. The stress of the first-order mode is only 0.6 MPa. Even if the material Poisson's ratio is 0.3, since the aspect ratio of the riser is 10^3, the influence of the Poisson's ratio on the cross-section is usually ignored.

Hypothesis 2 predominates in the modal vibration of the riser based on the pretension. The riser is similar to a tensioned string, so the propagation velocity of the axial vibration can be given as $C_{\text{Long}} = \sqrt{T/m_z}$ [29], where T is the pretension, m_z is the mass per unit length, and the propagation velocity of the first-order mode lateral vibration is $C_{\text{Trans}} = \sqrt{\omega}(EI/m_z)^{1/4}$ [30], where ω is the natural circular frequency, EI is the bending stiffness. We take the 682.75 m riser of the Norwegian DeepWater Program [4] as an example. The specific parameters are listed in Sect. 4. The axial vibration propagation velocity is 74.5 m/s, while the first-order lateral vibration propagation velocity is 5.2 m/s. The axis vibration propagation velocity is much larger than the first-order lateral vibration propagation velocity. Even if the lateral vibration order reaches 10th order (high-order) [16], the lateral vibration propagation velocity gets 16.9 m/s, and the previous conclusion is still valid. If the low-order lateral vibration of the riser is studied [4], it can be considered that the axial vibration propagation time is instantaneous, and the axial inertial force can be ignored.

Next, the formula is derived below. Take two differential units in the riser and set them as prototype P and model M, respectively. The prototype P and the model M only have different lengths of the Z-axis, and the other parameters are the same, as shown in Fig. 1. The dynamic differential equations of prototype P are no longer listed.

Hypothesis: $\mathrm{d}X = \mathrm{d}Y = R\mathrm{d}Z$, where R is real constant.

Obviously, $u{=}v{=}w/R$, where u, v, and w are the displacements of the x, y, and z-axes, respectively.

The moment of the center of the differential unit is written as, taking M_y as an example, $\tau_{xz} * \frac{1}{2}\mathrm{d}X * \mathrm{d}Y * \mathrm{d}Z = \tau_{zx} * \frac{1}{2}\mathrm{d}Z * \mathrm{d}X * \mathrm{d}Y$, simplify $\tau_{xz} = \tau_{zx}$. Similarly, $\tau_{xy} = \tau_{yx}, \tau_{yz} = \tau_{zy}$. This is consistent

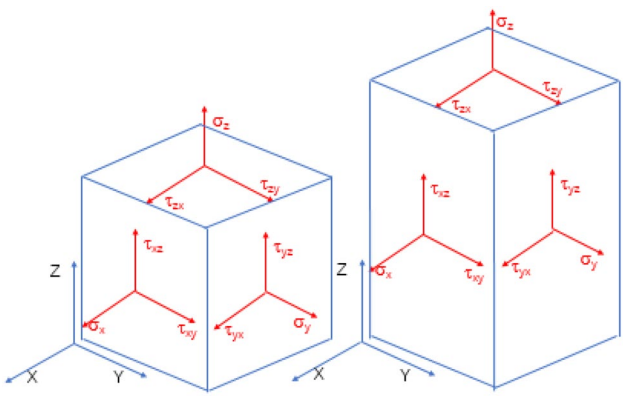

Fig. 1 The prototype P and the model M

with the theorem in Xu [31], that is, the shear stress acting on two mutually perpendicular planes and perpendicular to each other on the intersection of the two sides is equal (the same size, the same sign).

The differential equations of motion of model M are

$$\frac{\partial \sigma_x}{\partial x}+\frac{\partial \tau_{yx}}{\partial y}+\frac{\partial \tau_{zx}}{R\partial z}+f_x-\rho\frac{\partial^2 u}{\partial t^2}=0 \tag{1}$$

$$\frac{\partial \sigma_y}{\partial y}+\frac{\partial \tau_{zy}}{R\partial z}+\frac{\partial \tau_{xy}}{\partial x}+f_y-\rho\frac{\partial^2 v}{\partial t^2}=0 \tag{2}$$

$$\frac{\partial \sigma_z}{R\partial z}+\frac{\partial \tau_{xz}}{\partial x}+\frac{\partial \tau_{yz}}{\partial y}+f_z-\rho\frac{1}{R}\frac{\partial^2 w}{\partial t^2}=0 \tag{3}$$

From Eq. (1) and Eq. (2), we obtain.

$\tau_{zx,M}=R\tau_{zx,P}$, $\tau_{zy,M}=R\tau_{zy,P}$, $\tau_{yx,M}=\tau_{yx,P}$, $\sigma_{x,M}=\sigma_{x,P}$, $\sigma_{y,M}=\sigma_{y,P}$, where subscript P means the prototype of the riser, subscript M means the riser model.

The results of Eq. (1) and Eq. (2) are brought into Eq. (3), and both sides are multiplied by R to yield the following Eq. (4)

$$\frac{\partial \sigma_z}{\partial z}+R^2\frac{\partial \tau_{xz}}{\partial x}+R^2\frac{\partial \tau_{yz}}{\partial y}+Rf_z-\rho\frac{\partial^2 w}{\partial t^2}=0 \tag{4}$$

Only when $R=1$, the equation is established. However, $R=1$ means that the Z-axis has no scale, which does not match the results we want. According to the characteristics of the flexible riser, using hypothesis (2) to ignore the Z-axis inertial force in Eq. (4). Equation (4) can be written as

$$\frac{\partial \sigma_z}{\partial z}+R^2\frac{\partial \tau_{xz}}{\partial x}+R^2\frac{\partial \tau_{yz}}{\partial y}+Rf_z=0 \tag{5}$$

Further available obtain, $f_{z,M}=Rf_{z,P}$, $\sigma_{z,M}=R^2\sigma_{z,P}$. So the XY-direction is dynamically similar, while the Z-direction is only statically similar.

Elastic mechanics basically derives the scaled equation of the distorted model, and the following conclusions are given:

1. Under the underlying assumption, prototype P and model M can be dynamically similar through different length scales. Even if the length-diameter ratio of the flexible marine riser is 10^2–10^3, the length of the distortion model can be reduced.
2. The distortion model neglects the inertia force in the direction of distortion so that the direction only satisfies the static similarity. It shows that the basis of dynamic similarity in the dimensional analysis is the geometric similarity, which is still valid [32, 33]. The dynamic similarity of the X and Y directions provides sufficient support for the distortion model of the flexible riser.

3 Distortion model of flexible marine riser

Usually, researchers pay more attention to the lateral vibration of flexible marine risers rather than the axial vibration. The differential equations of the distortion model show that the lateral dynamics, along with the axial statics, is similar, which means only the similar requirement (or the scaling rule) of lateral vibration, not including axial vibration, of flexible marine risers is met. The modalities of lateral vibration are mainly studied. The lateral (radial) vibration governing equation of the riser [34]:

$$EI\frac{\partial^4 y(z,t)}{\partial z^4}-T\frac{\partial^2 y(z,t)}{\partial z^2}+m_z\frac{\partial^2 y(z,t)}{\partial t^2}=0 \tag{6}$$

where y is the radial displacement of the riser, z is the axial position of the riser, t is the time, EI is the bending stiffness, T is the pretension, and m_z is the mass per unit length.

$$m_z=m+m_A,\quad m_A=C_A m_a \tag{7}$$

where m is the mass, including both the riser structural body and the internal fluid, per unit length. As a crude approximation, the additional mass coefficient C_A is 1.0 [35]. Furthermore, m_a is the added mass per unit length. The mass ratio is $m^*=m/m_A$. According to Eq. (6), we can obtain the lateral vibration equation of the prototype P and the model M.

$$E_P I_P\frac{\partial^4 y_P(z,t)}{\partial z_P^4}-T_p\frac{\partial^2 y_P(z,t)}{\partial z_P^2}+m_{zP}\frac{\partial^2 y_P(z,t)}{\partial t_P^2}=0 \tag{8}$$

$$E_M I_M\frac{\partial^4 y_M(z,t)}{\partial z_M^4}-T_M\frac{\partial^2 y_M(z,t)}{\partial z_M^2}+m_{zM}\frac{\partial^2 y_M(z,t)}{\partial t_M^2}=0 \tag{9}$$

where subscript P means the prototype of the riser, subscript M means the riser model., L is the length of the riser, D is the diameter of the riser, and A is the cross-sectional area of the riser.

Bringing Eq. (8) into Eq. (9), we can obtain:

$$\lambda_E\lambda_I\frac{\lambda_y}{\lambda_L^4}\frac{\partial^4 y_M(z,t)}{\partial z_M^4}-\lambda_T\frac{\lambda_y}{\lambda_L^2}\frac{\partial^2 y_M(z,t)}{\partial z_M^2}+\lambda_{m_z}\frac{\lambda_y}{\lambda_t^2}\frac{\partial^2 y_M(z,t)}{\partial t_M^2}=0, \tag{10}$$

where λ_j represents the scale, j represents the physical quantity symbol, $j=E, I, L, T, m_z, t$. If Eq. (10) is established, which means:

$$\frac{\lambda_E\lambda_I}{\lambda_L^4}=\frac{\lambda_T}{\lambda_L^2}=\frac{\lambda_{m_z}}{\lambda_t^2} \tag{11}$$

If Eq. (11) is established, the lateral dynamic similarity of the riser is satisfied.

Taking the four basic variables, mass M_B, axial length L_B, radial length L_{DB}, time T_B, we can derive the four variables of the distorted model, the density of riser material ratio $\lambda_{\rho r}$, the elastic modulus of riser material ratio λ_E, the length direction (axial) ratio λ_L, the diameter direction (radial) ratio λ_D. The experimental fluid is freshwater. Eq. (11) can be written as:

$$\lambda_E \lambda_D^4 = \lambda_T \lambda_L^2 = \frac{\lambda_{m_z}}{\lambda_t^2} \lambda_L^4 \tag{12}$$

Using $m_z = m + C_A m_a = \rho A + \rho_w A_I + C_A \rho_w A_o$, λ_{m_z} yields

$$\lambda_{m_z} = \frac{\rho_P A_P + \rho_{wP} A_{IP} + C_A \rho_{wP} A_{oP}}{\rho_M A_M + \rho_{wM} A_{IM} + C_A \rho_{wM} A_{oM}} = \left(\frac{\lambda_{\rho r} + \frac{\rho_{wP}}{\rho_M} + \frac{\rho_{wP}}{\rho_M}}{1 + \frac{\rho_{wM}}{\rho_M} + \frac{\rho_{wM}}{\rho_M}} \right) \lambda_A = \left(\frac{\lambda_{\rho r} + \frac{\rho_{wP}}{\rho_M} + \frac{\rho_{wP}}{\rho_M}}{1 + \frac{\rho_{wM}}{\rho_M} + \frac{\rho_{wM}}{\rho_M}} \right) \lambda_D^2$$

where ρ is the density of the riser material, ρ_w is the density of water, A_I is the internal cross-section area of riser, A_O is the external cross-section area of riser, ρ_M is the density of the model material, ρ_{wM} is the density of freshwater, ρ_p is the density of the prototype material, and ρ_{wP} is the density of seawater.

Obviously, the system density ratio

$$\lambda_\rho = \frac{\lambda_{\rho r} + \frac{\rho_{wP}}{\rho_M} + \frac{\rho_{wP}}{\rho_M}}{1 + \frac{\rho_{wM}}{\rho_M} + \frac{\rho_{wM}}{\rho_M}} \tag{13}$$

Moreover, from Eq. (12), we can get time scale $\lambda_t = \lambda_L^2 / \lambda_D \sqrt{\lambda_\rho / \lambda_E}$, pretension scale $\lambda_T = \lambda_{m_z} \lambda_L^2 / \lambda_t^2 = \lambda_\rho \lambda_L^2 \lambda_D^2 / \lambda_t^2 = \lambda_E \lambda_D^4 / \lambda_L^2$.

Mode frequency scale [34] $\lambda_{f_n} = n/2\lambda_L \sqrt{(n\pi/\lambda_L)^2 \lambda_E \lambda_I / \lambda_{m_z} + \lambda_T / \lambda_{m_z}} = \lambda_t$, where n is the nth order mode number, 1,2,3,…. Longitudinal stress scale $\lambda_{\sigma_z} = \lambda_T / \lambda_A = \lambda_E \lambda_D^2 / \lambda_L^2$ and longitudinal strain scale $\lambda_\varepsilon = \lambda_{\sigma_z} / \lambda_E = \lambda_D^2 / \lambda_L^2$ can be obtained.

The complete similarity of the fluid is intricate to be achieved since the Reynolds number, *Re*, and the Froud number [5], *Fr*, are troublesome to satisfy at the same time. Usually, the dimensionless number *Fr*, which is the ratio of the inertial force to the mass force of the fluid, is easier to be satisfied when compared to *Re*. Although the influence of the gravity wave is usually considered, (especially considering the effect of the floating structure of the ship and the like by the wave load) it is not taken into account in this article, so the Froude number is ignored. As a result, the similar flow velocity, U, is calculated aiming the force similarity.

Because of the drag force scale $\lambda_{F_D} = \lambda_{\rho_w} \lambda_U^2 \lambda_L = 1.025 \lambda_U^2 \lambda_D$ (λ_{ρ_w} is the ratio of water in the prototype (seawater 1025 kg/m^3) to the water in the model (freshwater 1000 kg/m^3), which is 1.025.), the radial force scale is $\lambda_{FD} = \lambda_F \lambda_D / \lambda_L = \lambda_E \lambda_D^5 / \lambda_L^3$. So the flow speed scale is $\lambda_U = \lambda_D / \lambda_t = \lambda_D^2 / \lambda_L^2 \sqrt{\lambda_E / \lambda_{\rho w}}$. Note that the density scale is the fluid density scale $\lambda_{\rho w}$ rather than the model material density scale λ_ρ. In this way, drag force and dynamic response of fluid on the model are similar to that of the prototype.

In summary, the design flow of the riser distortion model can be obtained:

1. Establish the riser dynamics governing equation, use the distortion method to introduce four basic variables of M_B, L_B, L_{DB}, T_B, and design the distortion model to determine the parameter range;
2. According to the experimental conditions, select the appropriate experimental material and the value of the pretension applied to determine the optional experimental model. Experimental conditions such as site, instrument type, instrument measurement range;
3. The final experimental model is determined by comparing it with the riser prototype so as to appropriately present the dynamic characteristics of the riser prototype, and the corresponding numerical simulations could also be used to verify our model design.

Need to pay attention to the following conditions:

1. It is necessary to control the axial displacement of the experimental riser to prevent the axial displacement of the riser from being too large to apply the pretension of the design;
2. It is necessary to control the vertical joint force of the riser to be higher than zero, to prevent the buoyancy from being more significant than the combined force of the pretension and the weight, resulting in the distortion model floating;
3. When a larger distortion scale is used, the modal form of the distortion model differs from the modal form of the prototype. Compared with the order of the modal form of the prototype, the axial and torsional vibration forms of the natural vibration mode of the distortion model usually appear in the low-order mode. However, the structural dynamic response is generated by external load excitation. Even if the axial and torsional vibrations are in the low-order mode, the axial and torsional vibrations cannot participate in the structural dynamic response when there is no corresponding external load excitation. Even so, to avoid any coupling between the lateral bending, axial and torsional modes, the lower order modes of the riser distortion model should be lateral bending. Moreover, the frequencies of axial and/or torsional modes are higher than lateral bending modes. How to control the lateral bending vibration of the first several modes will be discussed in Sect. 4.1 below.

4 Numerical analysis

The 682.75 m riser of the Norwegian DeepWater Program [4] was taken as the prototype to carry out the distorted model scale design to verify the effectiveness of this method. The experimental model adopts a blue fiber plexiglass tube [36]. After comparison with the prototype structure parameters, the density scale is $\lambda_{\rho r} = 4.07$, the elastic modulus scale is $\lambda_E = 120000$, the axial direction length scale is $\lambda_L = 341.375$, and the transverse direction length scale is $\lambda_D = 35.56$. The fluid is freshwater with a density of 1000 kg/m^3. The prototype and model data are shown in Table 1.

The mass ratio is an important parameter affecting the fluid–solid coupling [37]. The mass ratio of the prototype is $m^* = 1.17$, and the mass ratio of the distorted model is $m^* = 1.11$. The error between the two is only 5.40%. The axial elongation of the distorted model is 6.78%, indicating that the axial pretension can be applied to the top of the riser model.

4.1 Selection of aspect ratio of distortion model

In the experimental design, the aspect ratio of the distortion model is an important parameter, which reflects the characteristics of the flexible riser and affects the model mode shape, which is related to whether the experiment can be implemented. To better select the appropriate length-diameter ratio of the distortion model, the relationship between the aspect ratio of the distortion model and the mode shape is plotted, as shown in Fig. 2. Figure 2 is calculated by ANSYS software based on the data in Table 1, taking into account the changes in the length and pretension. The beam element of Beam189 is used in the model, and the whole length is divided into 2000 beam elements. The boundary conditions are: the beam is hinged at both ends, and an axial constant pretension is applied at the top end of the model. The aspect ratio from 50 to 300, every step increase by 25. Furthermore, the first 30-order modes are obtained for each aspect ratio. The black rectangle represents lateral vibration, the red rectangle represents axial vibration, and the green rectangle represents torsional vibration.

First, look for the interval of the aspect ratio that can be used for the distortion experiment. The distortion model

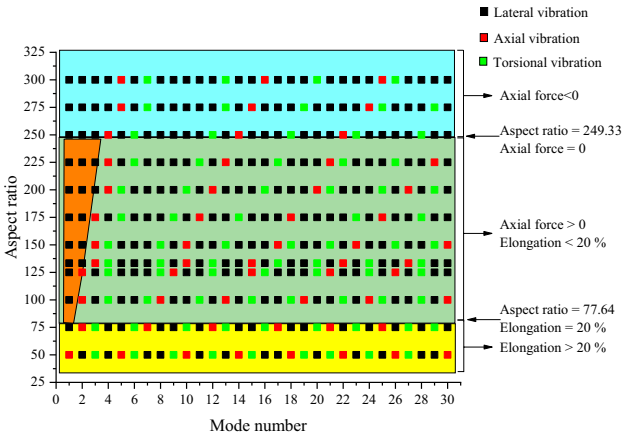

Fig. 2 The relation between aspect ratio and mode shape

aspect ratio affects the order of the mode shape, the amplitude of the pretension, and the length deformation of the model under the action of the pretension. When the aspect ratio is 77.64, the distortion model has an elongation of only 20% under the action of the pretension. When the aspect ratio is less than 77.64 (yellow part in Fig. 2), the elongation is further increased, causing the pretension to be unapplied, and the experimental model cannot be completed. When the aspect ratio is 249.33, the vertical force of the distortion model is 0, that is, the combined force of the pretension and buoyancy in the vertical direction is balanced with the weight of the model. When the aspect ratio is larger than 249.33 (light blue part in Fig. 2), the vertical force will be less than 0. Because the combined force of pretension and buoyancy is large, the distortion model cannot be fixed. Therefore, in the aspect ratio [77.64, 249.33] (dark green part of Fig. 2), the experiment can be successfully constructed.

The further analysis considers three factors: (1) the first-order of the distortion model should be dominated by lateral vibration, (2) the pretension of the distortion model should not be too small, (3) the elongation of the model should be small. The length–diameter ratio interval of the experimental model was further reduced. In the study of structural dynamics, the first few orders of vibration of the model are usually studied. For example, in the previous third-order vibration mode, the first third-order vibrations of the model are lateral

Table 1 Prototype and model data

Parameter	Length (m)	Tension (N)	Elastic modulus (N/m^2)	Density (kg/m^3)	Outer diameter/inner diameter (mm)
TTR prototype structure	682.75	4,000,000	2.07e11	7850	533.4/501.7
Scale	341.375	1,650,000	1.2e5	4.07	35.56
TTR distorted model	2	2.43	1.73e6	1928.7	15/14

vibration, axial vibration, and lateral vibration, respectively, from the long-diameter ratio of 77.64. As the aspect ratio increases gradually, when the aspect ratio is 120, the first third-order vibrations become lateral vibration, axial vibration, and lateral vibration. When the aspect ratio reaches 133.33, the first third-order vibration is lateral vibration, lateral vibration, and axial vibration. When the aspect ratio is 249.33, the first third-order vibrations are all lateral. As the aspect ratio increases, the lateral vibration gradually dominates the first third-order (the orange portion of Fig. 2).

Similarly, in the high-order vibration, the lateral vibration is dominant, and the axial vibration and the torsional vibration gradually move toward the higher order. In the first 30 modes, when the aspect ratio is 100, the number of lateral vibrations accounts for 53.33% of the total number of vibrations; when the aspect ratio is 233.33, the number of lateral vibrations accounts for 70% of the total number of vibrations, and the percentage of lateral vibration increases. The percentage of axial vibration and torsional vibration is reduced. Considering three factors comprehensively, the length-to-diameter ratio of this distortion model is 133.33, and the model length is 2 m. The specific data are shown in Table 1.

The modes obtained by the elastic calculation has the following characteristics: under a certain aspect ratio, the axial vibration frequency of each order and the lowest modal order of the axial vibration frequency exhibit an odd ratio, 1, 3, 5, …; the torsional vibration frequency of each order and the lowest mode order of the torsional vibration frequency shows a positive integer ratio, 1, 2, 3, 4, 5 …; the lateral vibration frequency of each order and the lowest modal order (first-order) of the lateral vibration frequency is not a positive integer ratio because the stiffness of the lateral vibrations includes bending stiffness and tensile stiffness (caused by pretension).

4.2 Modal numerical analysis

After designing the model, the modal similarities between the model and the prototype are discussed below. The modal similarity represents a similarity between the model and the prototype [38]. Figure 3 is a graph showing the 30° lateral natural frequency of the prototype riser and distortion model. Figure 4 shows the first three modal shapes of the prototype and the distorted model. It can be found that the third mode of the distorted model is axial vibration. Only lateral vibration is discussed here. It can be seen that the first-order natural frequency of the prototype riser is 0.055 Hz, and the 30-order natural frequency is only 2.24 Hz. The natural frequency of the first to 30th order increases linearly. The natural frequency of the prototype is low and dense, and the natural frequency difference between adjacent modes is small, thus generating high-order multi-mode broadband

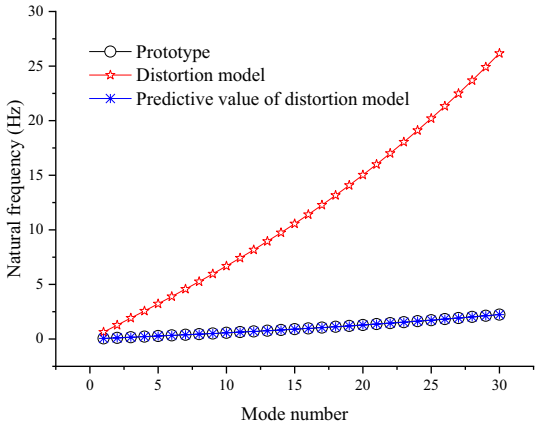

Fig. 3 Natural frequency

vibration. In the experimental model, the first-order natural frequency is 0.64 Hz, and the 30th order natural frequency is 26.17 Hz, and the natural frequency increases almost linearly from the first-order to the 30th order natural frequency.

Although the natural frequency of the distortion model is higher than the natural frequency of the prototype, it still retains the low and dense frequencies, and the difference between the natural frequency of adjacent modes is small, which allows high-order multi-mode broadband vibration could occur in the experiment. The predicted value of the distortion model is obtained by multiplying the natural frequency by the natural frequency ratio $\lambda_{fn}=\lambda_t=0.085$, which is equal to the natural frequency of the prototype, indicating that this method can achieve similar lateral dynamics.

It can be seen from Fig. 5, the ratio of pretension to bending stiffness contribution frequency of prototype riser decreases from 32.2 of the first-order vibration to 1.07 of thirtieth-order vibration, but it is always greater than 1, which has the characteristics of pretension dominating in natural frequency. The ratio of the pretension of the riser to the contribution frequency of bending stiffness is shown in Eq. (14). With the increase of mode order n, the ratio decreases. The distortion model coincides with the prototype in the graph completely, which satisfies the similarity of lateral dynamics.

$$\lambda_{f_{n,F/EI}}=\frac{\lambda_L}{n\pi}\sqrt{\frac{\lambda_F}{\lambda_E\lambda_I}} \tag{14}$$

where n is the mode number, 1,2,3,….

4.3 Pretension similarity analysis

The lateral vibration stiffness of the riser consists of the bending stiffness and tensile stiffness of the riser and is the composite stiffness. When the scale experiment is carried

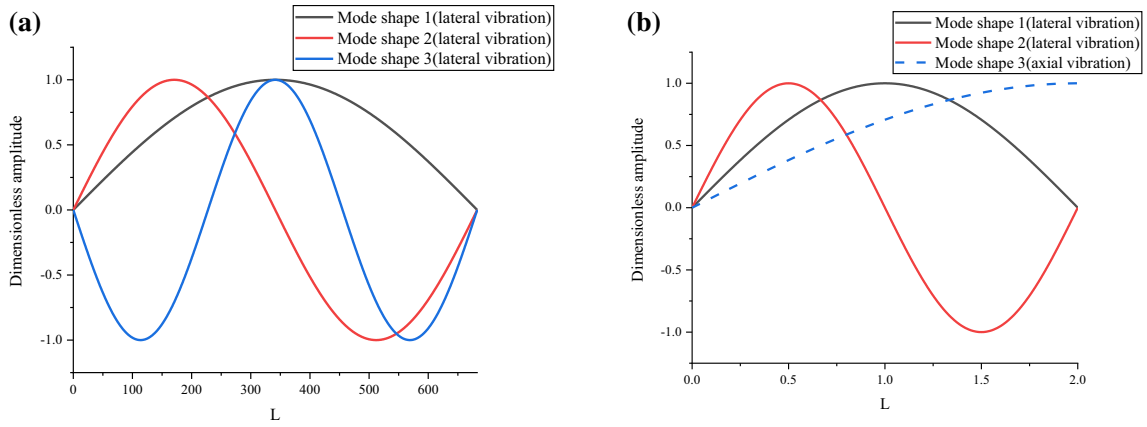

Fig. 4 **a**The first three mode shapes of prototype. **b** The first three mode shapes of distortion model

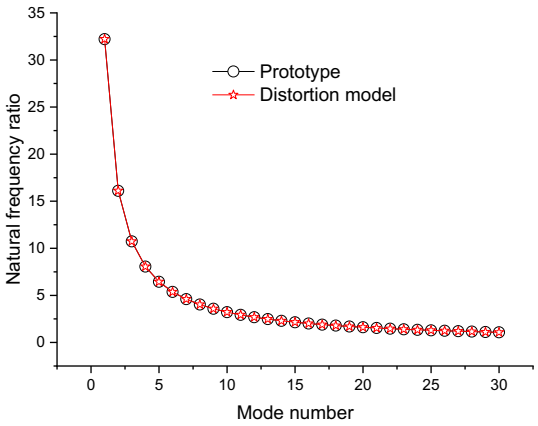

Fig. 5 Ratio of contribution frequency of riser pretension to bending stiffness

out, the pretension does not satisfy the similarity, which will have a non-negligible effect on the natural frequency of the model. The following example employs the model data from Ren et al. [39] for analysis. As shown in Table 2, the model scale ratio is 25 based on the similarity of the Froude number *Fr*, and the pretension ratio is 15,625. The ruler $\lambda_T = \lambda_E \lambda_D^4 / \lambda_L^2 = 625$ should be taken. It can be seen that the similar model is a special case of the distortion model. The ANSYS software is used to calculate the natural frequency of the prototype riser and the similar model. The element, mesh, and boundary conditions are the same as in the previous example. The riser does not consider the inflow mass and the additional mass.

Figure 6a shows the natural frequency of the prototype, the equal ratio model [39], and the distortion model. The natural frequency of the prototype is only 2.75 Hz at the 30th order. The 15th order is axial vibration, the 19th order is torsional vibration, and the remaining vibration forms are lateral vibration. The natural frequency of the distortion model is 69.612 Hz at 30th order, and the natural frequency has a distinct mutation at the 14th order because the 14th order of the mode is axial vibration. The natural frequency of the proportional model is 32.43 Hz in the 30th order, and the natural frequency has a sudden change in the 30th order because the 30th order of the mode is axial vibration. The pretension of the proportional model is smaller than the pretension of the distortion model, so the natural frequency of each mode is smaller than the natural frequency of the distortion model. The predicted value of the distortion model almost agrees with the prototype, and the predicted value of the equal ratio model is small compared to the prototype in Fig. 6a. However, in Fig. 6b, the predicted value of the proportional model is between 52.82% and 79.59% compared to the prototype, and the error gradually decreases as the model order increases. Because as the model order increases, the contribution of the bending stiffness in the lateral vibration gradually increases, while the contribution

Table 2 Basic parameters of prototype riser and its similar model (some parameters are taken from [39])

Parameter	Length (m)	Tension (N)	Elastic modulus (N/m^2)	Density (kg/m^3)	Outer diameter/inner diameter (mm)
TTR Prototype structure	1000	9,800,000	2.1e11	7800	508/457
Scale	25	625	1	1	25
Similar model	40	15,680	2.1e11	7800	20/18

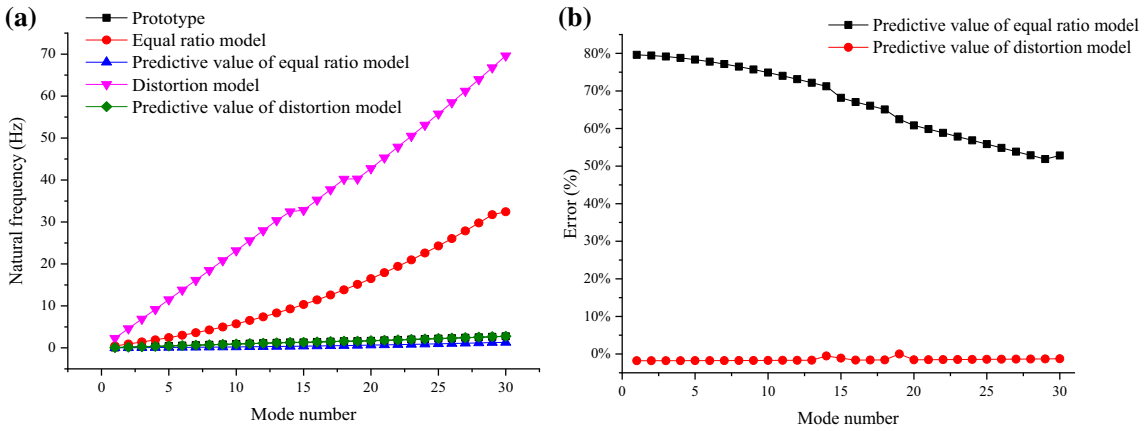

Fig. 6 **a** The natural frequencies of prototype, equal ratio model and distortion model, the predicted values. b The error of natural frequencies

of the pretension stiffness in the lateral vibration gradually decreases. The maximum error of the predicted model of the distortion model compared with the prototype is only −1.79%. The error comes from the elongation of the model under the pretension and the length of the model increases. The predicted value of the proportional model has a maximum error of 79.59%, and the minimum value exceeds 50%. It can be seen that the similarity of the pretension is a factor that cannot be ignored to satisfy the kinetic similarity.

4.4 Error analysis

In the numerical analysis, the design model is in good agreement with the dynamics of the prototype. However, for various reasons, there are errors in the design model and the experimental model, such as the material characteristic density, the elastic modulus, the magnitude of the pretension, and the like. This paper gives the influence of the error of pretension, elastic modulus, and material density on the natural frequency of the structure through the error analysis method. For simplicity, the assumed error values are −50%, −30%, −10%, 0%, 10%, 30%, 50%, ranging from −50% to 50%, and the range is sufficient to cover the actual model.

Figure 7a shows the influence of pretension on the natural frequency. The pretension values are calculated based on the relative error values. As the pretension increases, the natural frequency of the model increases in each mode, and the larger the amplitude of the pretension increase, the larger the vibration frequency value increases. In Fig. 7b, the relative error of the natural frequency is −29.21%, −16.26%, −5.07%, 4.95%, 14.08%, 22.53% at the first-order mode. In the 40th order mode, the relative errors of natural frequencies are −10.36%, −6.07%, −1.96%, 1.98%, 5.77%, and 9.43%, respectively. As the modal order increases, the relative error of the natural frequency under each pretension decreases, gradually moving closer to 0%, showing an asymmetric compression horn shape. The shape of the compression horn is produced because the pretension mainly controls the low-order modes, while the bending stiffness mainly controls the higher-order modes. As the modal order

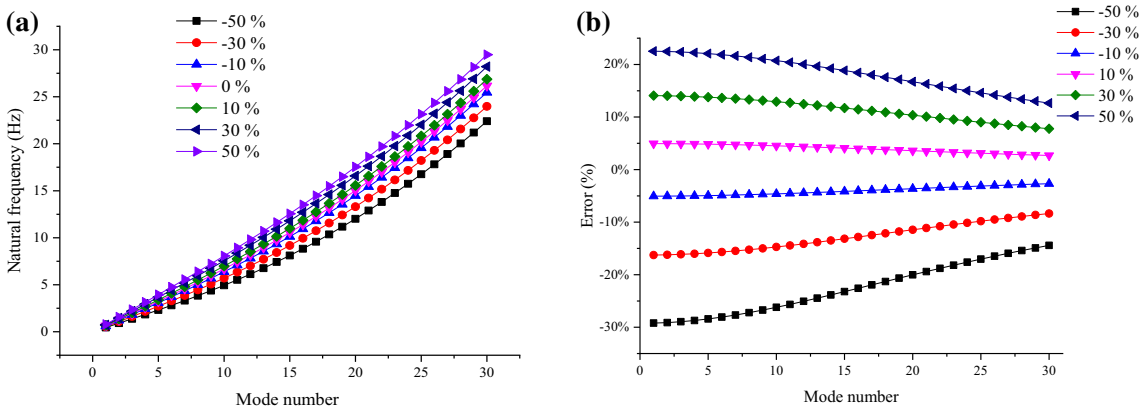

Fig. 7 **a** The influence of pretension on the natural frequency. **b** Pretension error vs. the natural frequency error

increases, the contribution of bending stiffness to natural frequencies increases, and the contribution of pretension to natural frequencies decreases. The asymmetrical shape is produced because the lateral vibration stiffness is the composite stiffness.

The effect of model material density on the natural frequency is given in Fig. 8a. In each mode, the natural frequencies almost coincide. In the 30th order mode in Fig. 8a, the vibration frequency is significantly different. In fact, the relative errors of each mode in Fig. 8b are the same, 2.75%, 1.62%, 0.53%, −0.52%, −1.55%, −2.54%, both less than 5%. The reason why the relative error caused by the material density is low is that the vibration system uses the system unit length density, and the system unit length density is the sum of the distortion model material unit length density and the distortion model drainage mass unit length density. According to Eq. (10), the fluid density ratio is usually 1.025 (the ratio of seawater density (1025 kg/m^3) to freshwater density (1000 kg/m^3)). When the material density ρ_M is small, the material density ratio λ_ρ is Large, so that the system density $\lambda_{\rho r}$ is not sensitive to the material density ρ_M.

Figure 9a shows the influence of the modulus of elasticity on the natural frequency. Based on the error value, the corresponding elastic modulus is calculated. In Fig. 9a, the natural frequencies of the first 15 stages are coincident, and the elastic modulus has little effect on the natural frequency. After the 15th order, the difference in the natural frequency becomes larger. With the increase of the modal order, the natural frequency of the model with different elastic modulus becomes larger, and the influence of the elastic modulus on the natural frequency is dominant. In Fig. 9b, the overall shape is umbrella-shaped, a little at the lower order mode, and spread at the higher order mode. In all models from the first to the 16th order mode, the error of the natural frequency is less than 5%. For the model with elastic modulus error of −30% and 30%, the error of the 23th natural frequency is less than 5%, and even for the 30th natural frequency the error is lower than 10%. In the 30th order mode,

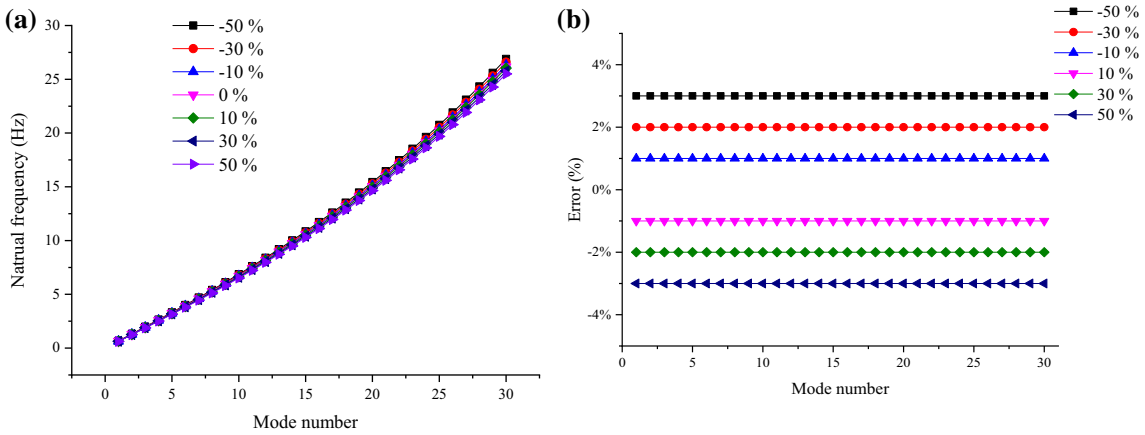

Fig. 8 **a**The influence of density on the natural frequency. **b** Density error vs. the natural frequency error

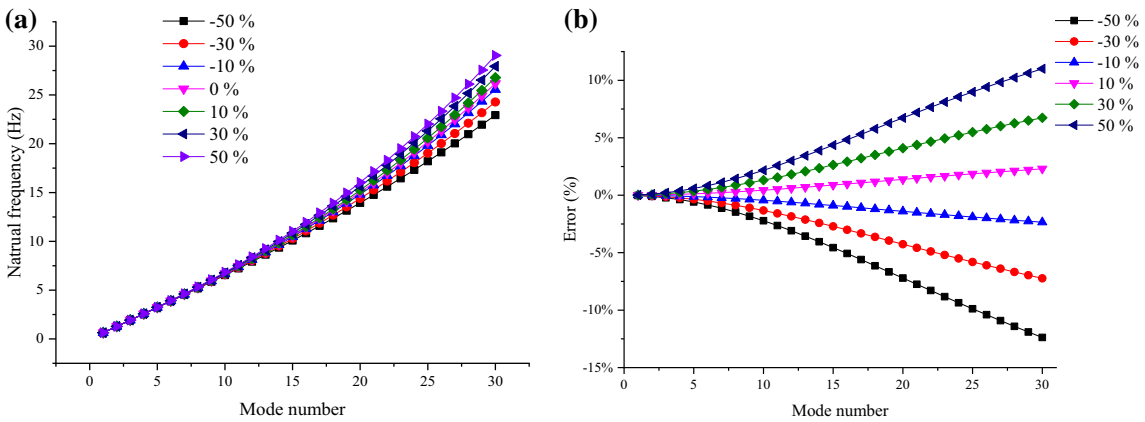

Fig. 9 **a** The influence of elastic modulus on the natural frequency. **b** Elastic modulus error vs. the natural frequency error

the natural frequency errors reach the maximum values (−12.38%, −7.23%, −2.35%, 2.30%, 6.74%, and 11.00%) since the contribution of bending stiffness to the natural frequency increases as the order of vibration increases.

It can be seen that the effects of errors in pretension, model density, and model elastic modulus on natural frequency cannot be ignored. To reduce the error of the natural frequency, the model parameters that have a significant influence on the natural frequency of the model are preferentially satisfied. For the three model parameters of pretension, model density, and model elastic modulus, the pretension is the most important in controlling the error between the prototype natural frequency and the model predicted natural frequency, so it is preferred. Second, it is the modulus of elasticity. Finally, the model density. The model density can change the mass ratio without significantly changing the natural frequency, which is beneficial to the same quality ratio of the model to the prototype.

5 Conclusions

In this paper, the feasibility of the theoretical formula of the distortion model is proved by the derivation of the dynamic differential equation in elastic mechanics. Based on the dynamic differential equation of the distorted model, a design method of the distorted model is proposed for the deep sea flexible riser. In the numerical analysis, the distortion model design of an actual deep-sea flexible riser was carried out, and the aspect ratio, modality, pretension, error, etc. were discussed, and the following conclusions were obtained.

1. The lateral direction of the distortion model of the deep sea flexible riser satisfies the similarity of the dynamics, and the longitudinal direction satisfies the static similarity.
2. The distortion model solves the problems that the aspect ratio of the riser is as high as 10^3, and it is difficult to equal the scale, and pretension is not satisfied with the kinetic similarity. The prototype and model scales are given, lateral displacement ratio ruler λ_D, longitudinal displacement ratio ruler λ_L, pretension ratio ruler $\lambda_T = \lambda_E \lambda_D^4 / \lambda_L^2$, time scale ruler $\lambda_t = \left(\lambda_L^2 / \lambda_D\right) \sqrt{\lambda_\rho / \lambda_E}$, inflow speed ratio ruler $\lambda_U = \left(\lambda_D^2 / \lambda_L^2\right) \sqrt{\lambda_E / \lambda_{\rho w}}$, and the like.
3. The distortion model aspect ratio affects the order of the mode shape, the amplitude of the pretension, and the length deformation of the model under the action of the pretension. Three factors need to be considered comprehensively to select a reasonable distortion model aspect ratio. The first few vibrations of the model are mainly in the transverse direction, whether the pretension application is convenient, and the elongation of the model under the pretension is small.
4. When there is an error in the model, it will affect the natural frequency. When the parameter range is −50%–50%, the maximum error is when the pretension is −50%, and the first-order natural frequency error is −29.21%; When the elastic modulus is −50%, the 30th order natural frequency error is −12.38%; and when the density is −50%, the natural frequency error of each order is 2.75%. Therefore, the model parameters should be preferential of high to low: pretension, model elastic modulus, and model density.

The distortion model experimental design method provides new ideas for other marine structures such as mooring and catenary risers. Future work can be further verified by experimental methods to determine the rationality of this method.

Acknowledgements This work is supported by the Strategic Priority Research Program of the Chinese Academy of Sciences (Grant No. XDA22000000).

References

1. Chen WM, Fu YQ, Guo SX, Jiang CH (2017) Review on fluid-solid coupling and dynamic response of vortex-induced vibration of slender ocean cylinders. Adv Mech 47:201703. https://doi.org/10.6052/1000-0992-16-005
2. Wu XD, Ge F, Hong YS (2012) A review of recent studies on vortex-induced vibrations of long slender cylinders. J Fluid Struct 28:292–308. https://doi.org/10.1016/j.jfluidstructs.2011.11.010
3. VIVDR (2008) Vortex induced vibration data repository. 2008 [cited 2019 1012]. Available from http://web.mit.edu/towtank/www/vivdr/index.html
4. Kaasen KE, Lie H, Solaas F, Vandiver JK (2000) Norwegian Deepwater Program: analysis of vortex-induced vibrations of marine risers based on full-scale measurements. In: Offshore Technology Conference, 1–4 May, Houston, Texas
5. Huse E (1996) Experimental investigation of deep sea riser interaction. In: Offshore Technology Conference, 6–9 May, Houston, Texas
6. Huse E, Kleiven G, Nielsen FG (1998) Large scale model testing of deep sea risers. In: Offshore Technology Conference, 4–7 May, Houston, Texas
7. Huse E, Kleiven G, Nielsen FG (1999) VIV-induced axial vibrations in deep sea risers. In: Offshore Technology Conference, 3–6 May, Houston, Texas
8. Yin D, Lie H, Russo M, Grytøyr G (2018) Drilling riser model test for software verification. J Offshore Mech Arct Eng 140(1):011701. https://doi.org/10.1115/1.4037727
9. Allen DW, Liu N (2017) VIV suppression device development and the perils of Reynolds number. In: ASME 2017 36th international conference on ocean, offshore mechanics and arctic engineering, 25–30 June, Trondheim, Norway
10. Denney D (2006) High-mode-number vortex-induced-vibration field experiments. J Petro Technol 58(02):69–70. https://doi.org/10.2118/0206-0069-jpt

11. Vandiver JK, Allen D, Li L (1996) The occurrence of lock-in under highly sheared conditions. J Fluid Struct 10(5):555–561. https://doi.org/10.1006/jfls.1996.0037
12. Allen DWD, Henning DL (2001) Prototype vortex-induced vibration tests for production risers. In: Offshore technology conference, 30 April–3 May, Houston, Texas
13. Hong S, Choi YR, Park JB, Park YK, Kim YH (2002) Experimental study on the vortex-induced vibration of towed pipes. J Sound Vib 249(4):649–661. https://doi.org/10.1006/jsvi.2001.3858
14. Tognarelli MA, Slocum ST, Frank WR, Campbell R B (2004) VIV response of a long flexible cylinder in uniform and linearly sheared currents. In: Offshore technology conference, 3–6 May, Houston, Texas
15. Chaplin JR, Bearman PW, Huera-Huarte FJ, Pattenden RJ (2005) Laboratory measurements of vortex-induced vibrations of a vertical tension riser in a stepped current. J Fluid Struct 21(1):3–24. https://doi.org/10.1016/j.jfluidstructs.2005.04.010
16. Vandiver JK (2003) High mode number VIV experiments. In: IUTAM symposium on integrated modeling of fully coupled fluid structure interactions using analysis. Springer, Dordrecht.
17. Vandiver JK, Marcollo H, Swithenbank S, Jhingran V (2013) High mode number vortex-induced vibration field experiments. In: Offshore technology conference, 2–5 May, Houston, Texas.
18. Swithenbank SB (2007) Dynamics of long flexible cylinders at high-mode number in uniform and sheared flows. Dept. of Mechanical Engineering. Massachusetts Institute of Technology
19. Luo Z, Zhu YP, Zhao XY, Wang DY (2016) Determining dynamic scaling laws of geometrically distorted scaled models of a cantilever plate. J Eng Mech 142(4):04015108. https://doi.org/10.1061/(Asce)Em.1943-7889.0001028
20. Baker WE, Westine PS, Dodge FT (1973) Similarity methods in engineering dynamics. Hayden Book Company. Inc., Rochelle Park, New Jersey
21. Simitses GJ, Starnes JH, Rezaeepazhand J (2001) Structural similitude and scaling laws for plates and shells: a review. In: Durban D, Givoli D, Simmonds JG (eds) Advances in the mechanics of plates and shells. Springer, Netherlands, Dordrecht, pp 295–310
22. Rezaeepazhand J, Simitses GJ, Starnes JH (1995) Use of scaled-down models for predicting vibration response of laminated plates. Compos Struct 30(4):419–426. https://doi.org/10.1016/0263-8223(94)00064-6
23. Rezaeepazhand J, Simitses GJ (1996) Design of scaled down models for predicting shell vibration repsonse. J Sound Vib 195(2):301–311. https://doi.org/10.1006/jsvi.1996.0423
24. Adams C, Bos J, Slomski EM, Melz T (2018) Scaling laws obtained from a sensitivity analysis and applied to thin vibrating structures. Mech Syst Signal Pr 110:590–610. https://doi.org/10.1016/j.ymssp.2018.03.032
25. Franco F, Berry A, Petrone G, De Rosa S, Ciappi E, Robin O (2020) Structural response of stiffened plates in similitude under a turbulent boundary layer excitation. J Fluid Struct 98:103119. https://doi.org/10.1016/j.jfluidstructs.2020.103119
26. Luo Z, Li L, He FX, Yan XL (2021) Partial similitude for dynamic characteristics of rotor systems considering gravitational acceleration. Mech Mach Theory 156:104142. https://doi.org/10.1016/j.mechmachtheory.2020.104142
27. Casaburo A, Petrone G, Franco F, De Rosa S (2019) A review of similitude methods for structural engineering. Appl Mech Rev 71(3). https://doi.org/10.1115/1.4043787
28. Brekke J, Chakrabarti S, Halkyard J (2005) Drilling and production risers. In: Chakrabarti SK (ed) Handbook of offshore engineering. Elsevier, Amsterdam, pp 709–859
29. Rao ZB (2015) The flow of power in the vortex-induced vibration of flexible cylinders. Department of Mechanical Engineering, Massachusetts Institute of Technology
30. Doyle JF (1989) Wave propagation in structures. Wave propagation in structures. Springer, New York, pp 126–156
31. Xu ZL (2016) Elasticity (5th edn). Higher Education Press, Beijing
32. Chakrabarti SK (2005) Physical modelling of offshore structures. In: Handbook of offshore engineering. Elsevier, pp 1001–1054
33. Oshiro RE, Alves M (2012) Predicting the behaviour of structures under impact loads using geometrically distorted scaled models. J Mech Phys Solids 60(7):1330–1349. https://doi.org/10.1016/j.jmps.2012.03.005
34. Vandiver JK, Li L (2005) Shear7 V4. 4 program theoretical manual. Massachusetts Institute of Technology
35. Williamson CHK, Govardhan R (2004) Vortex-induced vibrations. Annu Rev Fluid Mech 36(1):413–455. https://doi.org/10.1146/annurev.fluid.36.050802.122128
36. Zhang YB (2011) Research on vortex-induced vibration prediction and vibration suppression technology of deep sea infusion riser in Ocean University of China. Ocean University of China
37. Khalak A, Williamson CHK (1999) Motions, forces and mode transitions in vortex-induced vibrations at low mass-damping. J Fluid Struct 13(7–8):813–851. https://doi.org/10.1006/jfls.1999.0236
38. Luo Z, Zhu YP, Zhao XY, Wang DY (2015) High-order vibrations' dynamic scaling laws of distorted scaled models of thin-walled short cylindrical shells. Mech Based Des Struc 43(4):514–534. https://doi.org/10.1080/15397734.2015.1044610
39. Ren T, Fu SX, Li RP, Yang JM (2011) Full scale riser vortex-induced-vibration responseprediction based on model test. J Ship Mech 15:364–370. https://doi.org/10.3969/j.issn.1007-7294.2011.04.006